Local Weak Ferromagnetism in Single-Crystalline Ferroelectric BiFeO_{3}

M. Ramazanoglu, M. Laver, W. Ratcliff, II, S. M. Watson, W. C. Chen, A. Jackson, K. Kothapalli, Seongsu Lee, S.-W. Cheong, and V. Kiryukhin

Phys. Rev. Lett. **107**, 207206 — Published 11 November 2011

DOI: 10.1103/PhysRevLett.107.207206

Local weak ferromagnetism in single-crystalline ferroelectric $BiFeO_3$

M. Ramazanoglu,[1] M. Laver,[2-4] W. Ratcliff II,[5] S. M. Watson,[5] W.C. Chen,[4,5]
A. Jackson,[4,5] K. Kothapalli,[4,5] Seongsu Lee,[6] S.-W. Cheong,[1] and V. Kiryukhin[1]

[1]*Department of Physics and Astronomy,*
Rutgers University, Piscataway, New Jersey 08854, USA

[2]*Materials Research Division, Risø DTU,*
Technical University of Denmark, DK-4000 Roskilde, Denmark

[3]*Nano Science Center, Niels Bohr Institute,*
University of Copenhagen, DK-2100 Copenhagen, Denmark

[4]*Department of Materials Science and Engineering,*
University of Maryland, College Park, Maryland 20742, USA

[5]*NIST Center for Neutron Research,*
National Institute of Standards and Technology,
Gaithersburg, Maryland 20899, USA

[6]*Neutron Science Division, Korea Atomic Research Institute, Daejon 305-353, Korea*

Abstract

Polarized small-angle neutron scattering studies of single-crystalline multiferroic $BiFeO_3$ reveal a long-wavelength spin density wave generated by $\sim 1^\circ$ spin canting of the spins out of the rotation plane of the antiferromagnetic cycloidal order. This signifies weak ferromagnetism within mesoscopic regions of dimension 0.03 microns along $[1\bar{1}0]$, to several microns along [111], confirming a long-standing theoretical prediction. The average *local* magnetization is 0.06 μ_B/Fe. Our results provide an indication of the *intrinsic* macroscopic magnetization to be expected in ferroelectric $BiFeO_3$ thin films under strain, where the magnetic cycloid is suppressed.

PACS numbers: 75.85.+t, 75.25.-j, 61.05.fg

Magnetoelectric (ME) multiferroics capture attention of researchers on account of their prospective applications, such as multistate memory and spintronics, as well as the unusual effects (hybrid excitations, linear ME effect) exhibited by these materials.[1] For many purposes, an "ideal" compound would combine coupled ferroelectric (FE) and ferromagnetic (FM) orders in a single phase, at room temperature. Despite significant efforts, unambiguous observation of such a system has yet to be reported. Among the known multiferroics, $BiFeO_3$ (BFO) shows the most promise for fulfilling the above requirements.[2] At room temperature, it is a rhombohedral $R3c$ perovskite with a large electric polarization $\mathbf{\Pi}\approx 90$ $\mu C/cm^2$ pointing along the elongated [111] direction of its pseudo-cubic unit cell ($a = 3.96$ Å, $\alpha = 89.4°$). In bulk BFO, the Fe^{3+} spins order in a G-type antiferromagnetic structure with a superimposed long-wavelength (∼620 Å) cycloidal modulation.[3, 4] The modulation can propagate along any of the 3 symmetry-equivalent wavevectors $\boldsymbol{\tau}_1=\delta$[1,-1,0], $\boldsymbol{\tau}_2=\delta$[1,0,-1], and $\boldsymbol{\tau}_3=\delta$[0,-1,1], where δ=0.0045 reciprocal lattice units (r.l.u.), forming 3 distinct magnetic domains within a single FE domain.[3, 5, 6] The spins rotate in the plane defined by the normal vectors [111] and $\boldsymbol{\tau}$, see Fig. 1(a). The orientation of this plane can be controlled with an applied electric field by switching the direction of $\mathbf{\Pi}$, accentuating the potential of BFO for applications involving ME effects.[5, 7] The cycloidal modulation can be suppressed into a homogeneous G-type state by anisotropic strain, as observed in certain BFO thin films[2], or by large magnetic fields in bulk samples.[8, 9]

The symmetry of bulk BFO permits a magnetoelectric interaction with a similar form to the Dzyaloshinski-Moriya case that leads to the spin canting producing a weak FM moment $\mathbf{m}\sim\mathbf{\Pi}\times\mathbf{L}$, where $\mathbf{L}$ is the antiferromagnetic vector.[8, 10] For the spin structure described above, $\mathbf{m}$ is perpendicular to both the [111] and $\boldsymbol{\tau}$ vectors. The magnitude of $\mathbf{m}$ is proportional to the projection of $\mathbf{L}$ on the $\boldsymbol{\tau}$ direction. In the pure G-type state, this leads to a uniform FM magnetization, with a theoretically predicted magnitude in the 0.02-0.1 μ_B/Fe range (μ_B is Bohr magneton).[10, 11] A linear ME effect is also predicted in this state.[8, 10, 11] Motivated by these predictions, significant efforts have been devoted to search of the FM moment in G-type BFO thin films.[2] To date, the results are inconclusive, with some groups reporting moments as large as 1 μ_B/Fe,[12] while others concluding that any possible intrinsic magnetization is 2 orders of magnitude smaller, or even undetectable.[13, 14] Clearly, resolution of this controversy is important for further work on ferromagnetic ferroelectrics.

In bulk BFO, the cycloidal modulation converts the uniform FM into a spin density wave (SDW) of the same wavelength ∼620 Å, as shown in Fig. 1(a). This state exhibits neither a bulk spontaneous magnetization nor a linear ME effect.[8] However, its characterization is clearly of vital importance for the estimation of the possible intrinsic FM moment in films, as well as for the understanding of many of the intriguing properties of the bulk material. The spin tilts producing the predicted SDW are coupled ferromagnetically in the directions normal to $\boldsymbol{\tau}$. Therefore, they should produce magnetic Bragg reflections at scattering vectors $\mathbf{q} = \mathbf{0} \pm \boldsymbol{\tau}_i$. Because the cycloidal modulation is superimposed on the G-type antiferromagnetic structure in which the nearest-neighbor spins are antialigned, its magnetic reflections are shifted from this $\mathbf{q}$ by [0.5,0.5,0.5] and do not overlap with the SDW signal. Here we use small-angle neutron scattering (SANS) to probe this region in bulk single crystals, and explore the nature of the predicted SDW with neutron polarization analysis.

A 1×1×3 mm^3 $BiFeO_3$ single crystal was grown using the flux method.[5] The high quality of the sample was confirmed by neutron diffraction and bulk magnetization measurements.[15] The unique [111] axis was determined, and the FE monodomain sample composition confirmed, using the BT-9 diffractometer at the NIST Center for Neutron Research (NCNR). SANS measurements were performed at room temperature on the NG3-SANS instrument at the NCNR, using both polarized and unpolarized neutrons of mean wavelength $\lambda = 7.5$ Å. Incident neutrons were polarized using a Fe/Si transmission polarizer and the final neutron spin state was analyzed using a cell of nuclear-spin-polarized ^{3}He.[16] Magnetic guiding fields were used to maintain the neutron polarization $\mathbf{P}$ along the path between polarizer and analyzer. We employ two setups with $\mathbf{P}$ at the point of scattering either parallel or perpendicular to the beam using correspondingly directed fields of 3.5 mT and 1 mT respectively at the sample position. The measured intensity was normalized to the known neutron flux and sample volume to obtain absolute units. In this work, error bars are from counting statistics, and represent one standard deviation.

Figs. 1(b) and (c) show the scattering observed with the incident beam roughly parallel to [111]. Six Bragg spots in the directions coinciding with $\pm\boldsymbol{\tau}_i$ (as determined on BT-9) are plainly visible. The figures are constructed by summing the detector images measured by rocking each of the 6 spots through the Bragg condition along the shortest path through the Ewald sphere. The rocking angle is referred to as β below. The periodicity of the structure giving rise to the spots is 624±3 Å, as extracted from the $|\mathbf{q}|$-dependence of the

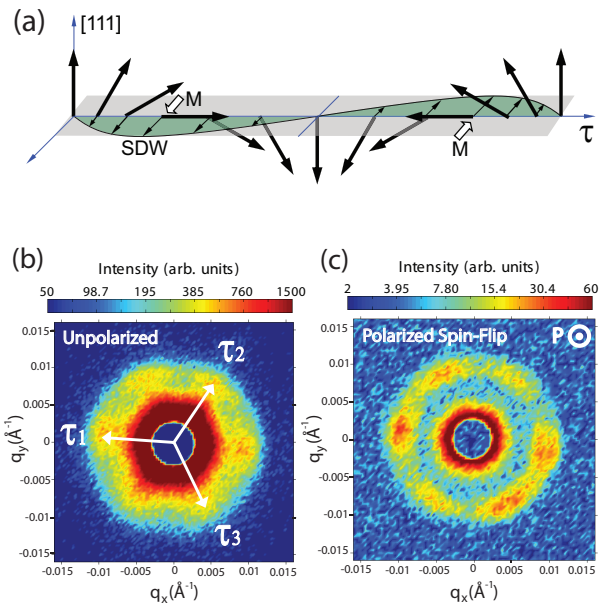

FIG. 1: (color online). (a) The SDW (thin arrows normal to both [111] and $\boldsymbol{\tau}$) produced by the tilt of the Fe spins out of the plane of the magnetic cycloid (thick arrows in the plane defined by [111] and $\boldsymbol{\tau}$). The amplitude of the SDW is exaggerated. Only a few representative spins are shown. Open arrows show local magnetization due to the SDW. (b) and (c) Images of the diffraction pattern in the (111) scattering plane with (b) unpolarized neutrons, (c) neutrons polarized with $\mathbf{P} \parallel$ beam that scatter with spin flip. The images were prepared by summing several detector measurements over a range of rocking angles β (see text), allowing all Bragg reflections from the long-wavelength modulation to be presented in a single image. A beamstop blocks the direct beam in the center of each image.

azimuthally-averaged intensity shown in Fig 2(a). It matches the periodicity of the magnetic cycloid. The 6 Bragg spots are consistent with the anticipated SDW signal, provided that all 3 magnetic domains are present giving $\pm\boldsymbol{\tau}_i$, i=1-3. The domain populations obtained from the integrated intensities of the peaks are 39%, 27%, and 34% (all $\pm$1%), in agreement with the cycloidal domain populations obtained using wide-angle diffraction in the vicinity of the G-type [0.5,0.5,0.5] position.

To establish the origin of the scattering at $\boldsymbol{\tau}_i$, longitudinal polarization analysis was carried out. For an ensemble of atoms at positions $\mathbf{r}_j$, with atomic scattering length b_j and

magnetic moment $\mathbf{S}_j$, the scattered intensities are [17]

$$I^{\pm\pm} \propto \sum_{jl} \mathrm{e}^{-\mathrm{i}\mathbf{q}\cdot(\mathbf{r}_j-\mathbf{r}_l)} \left[b_j b_l^* + Z_j Z_l^* \pm (Z_j b_l^* + b_j Z_l^*)\right] \quad (1)$$

$$I^{\pm\mp} \propto \sum_{jl} \mathrm{e}^{-\mathrm{i}\mathbf{q}\cdot(\mathbf{r}_j-\mathbf{r}_l)} \left[X_j X_l^* + Y_j Y_l^* \mp \mathrm{i}\hat{\mathbf{z}}\cdot(\mathbf{T}_j \wedge \mathbf{T}_l^*)\right] \quad (2)$$

describing non-spin-flip (nsf) and spin-flip (sf) scattering, respectively. Neutrons probe only the components of $\mathbf{S}$ that are perpendicular to the scattering vector $\mathbf{q}$; this is described by the quantity $\mathbf{T} = (X, Y, Z) \propto \mathbf{S} - (\mathbf{S}\cdot\hat{\mathbf{q}})\hat{\mathbf{q}}$, where the neutron polarization direction $\hat{\mathbf{P}}$ fixes the Cartesian $\hat{\mathbf{z}}$-axis. The nsf channels (1) contain both magnetic and nuclear scattering, while the sf channels (2) contain only magnetic scattering. Collecting data in all 4 channels permits correction for the leakage of the "wrong" polarization,[18] characterized by the flipping ratio ≈16 of our setup. This is done in Figs. 2 and 3. We note that after this correction, the scattering for $q \to 0$ [Fig. 1(b)] is only present in the nsf channel, *i.e.* it is nonmagnetic. It follows a power law $I \propto q^{-d}$ with $d \simeq 4$, consistent with a Porod regime of scattering, where $q \gg 1/D$, probably from crystal grain boundaries on scales $D \gg 300\,\text{Å}$.

For $\hat{\mathbf{P}} \parallel$ beam, the sf channel picks up only the moment normal to both [111] and $\boldsymbol{\tau}$. The nsf channel contains the intensity due to the moment parallel to [111], as well as nuclear scattering. Figs. 1(c), 2(b) and (c) show that the Bragg peaks are present only in the sf channel. These data show that (i) the signal at $\boldsymbol{\tau}_i$ is purely magnetic, (ii) it is produced by the spin component normal to both $\boldsymbol{\tau}$ and [111], as in the SDW of Fig. 1(a), and (iii) the magnetic cycloid does not contribute to scattering at this $\mathbf{q}$, as expected. (As shown in Fig. 1(a), the cycloid is confined in the plane defined by [111] and $\boldsymbol{\tau}$, and therefore would only scatter in the nsf channel in this geometry.) To our knowledge, this is the first demonstration of the spin component normal to the cycloid plane (spin canting) in BFO.

The rocking scans in Fig. 2(b) probe spin-spin correlations along the [111] direction. They are well described by the Lorentzian shape, giving the correlation length l=3.3±0.2 μm for the exponentially decaying correlations. The peak width in the radial direction (parallel to $\boldsymbol{\tau}$) is strongly coupled to l and given by $a/\sqrt{1+(aql)^2}$, where a=0.095° is the angular spread of the beam. The close agreement of this notional value with the observed width is shown in Fig. 2(a). In the azimuthal direction, the intrinsic width of the Bragg spots is 11±2°. This might result from a ∼10° spread in the direction of the cycloid modulation wave vector in the (111) plane, as proposed in Ref. [3]. Alternatively, this could indicate a

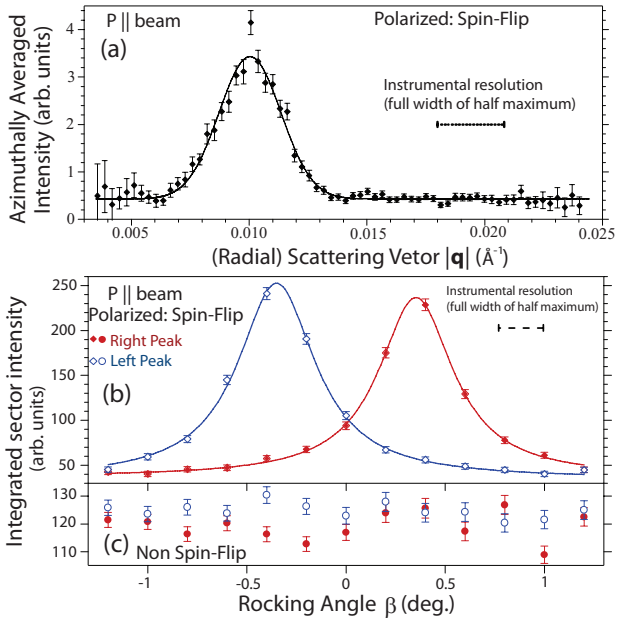

FIG. 2: (color online). Details of the $\pm\boldsymbol{\tau}_1$ diffraction spots [left and right spots in Figs. 1(b) and (c)], using neutrons polarized with $\mathbf{P} \parallel$ beam. Corrections for the polarizing efficiency of the instrument have been included. (a) $|\mathbf{q}|$-dependence of azimuthally averaged intensity through both left and right spots at the peaks of their rocking curves. The solid line depicts a Gaussian fit. (b) and (c) Rocking curves for both left and right spots in the sf (b) and nsf (c) channels. The solid lines are Lorentzian fits. The dashed and dotted bars in these figures illustrate aspects of the experimental resolution discussed in the text. 55°-wide sectors on the detector were used to pick out the $\pm\boldsymbol{\tau}_1$ spots; similar results may be obtained with smaller sectors and/or by examining another pair of diffraction spots $\pm\boldsymbol{\tau}_2$, $\pm\boldsymbol{\tau}_3$.

$\sim$0.1 μm correlation length in the direction normal to the plane of the cycloid.

To make a quantitative estimate of the spin components, we use a setup with $\mathbf{P} \perp$ beam, in which Bragg peaks are present in both sf and nsf data. In this geometry, $\mathbf{T} = (X, Y, Z) = (\mu\cos\alpha, \nu, \mu\sin\alpha)$, where μ is a spin component normal to the plane of the cycloid (the SDW), ν is that along [111], and α is the angle between $\boldsymbol{\tau}$ and $\mathbf{P}$, see Fig. 3(a). The terms $X_j X_l^*$, $Y_j Y_l^*$, and $Z_j Z_l^*$ in Eqs. (1) and (2) are accordingly proportional to $\mu^2\cos^2\alpha$, ν^2, and $\mu^2\sin^2\alpha$, respectively. In Fig. 3(b), the intensity integrated over the rocking curve of each Bragg spot $\boldsymbol{\tau}_i$ is plotted versus α, after normalizing for the relative domain populations.

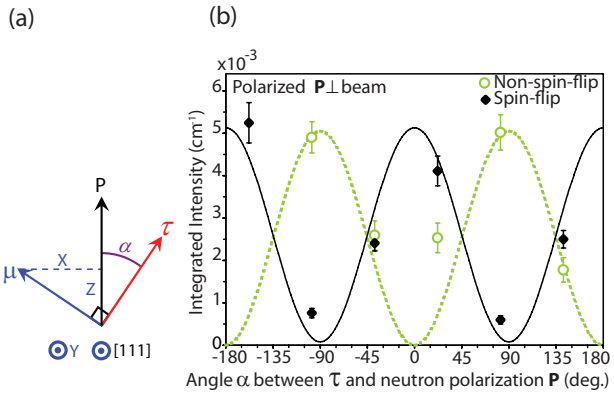

FIG. 3: (color online). Data for neutrons polarized with $\mathbf{P} \perp$ beam, in the vertical direction on the detector. (a) Schematic in detector plane illustrating the relationship between $\mathbf{P}$, $\boldsymbol{\tau}$, and the components (X, Y, Z) of the vector $\mathbf{T}$ associated with the magnetic modulation. (b) Dependence on the angle α between $\boldsymbol{\tau}$ and $\mathbf{P}$ of the polarized neutron intensities for all Bragg spots $\pm\boldsymbol{\tau}_i$, each integrated over its rocking curve and normalized by its relative domain population. Both the sf and nsf channels are shown. The lines are fits described in the text.

Curves of the form $A\sin^2\alpha$ and $A\cos^2\alpha + B$, where $A \propto \mu^2$ and $B \propto \nu^2$, are fitted to the nsf and sf data, respectively. In agreement with the $\mathbf{P} \parallel$ beam data of Fig 2, we obtain ν=0 within experimental accuracy (B is less than 2% of A). In absolute units, the data of Fig. 3(b) give I=0.0050±0.0003 cm^{-1} for the integrated intensity of the magnetic Bragg peak. This intensity is equal to

$$I = \frac{\lambda^3}{\sin 2\theta_B}\left(\frac{gS_{max}}{V}\frac{\gamma r_0}{2}|F_A(\boldsymbol{\tau})|\right)^2 |F_S(\boldsymbol{\tau})|^2 \qquad (3)$$

where $\gamma r_0/2$=2.7×10$^{-13}cm/\mu_B$, $2\theta_B$ is the scattering angle, $g = 2$ for spin-only scattering from Fe^{3+} ions whose normalized magnetic form factor $F_A \simeq 1$ at low $\mathbf{q}$, S_{max} is the amplitude of the SDW, and F_S=0.5 is the normalized form factor of the sinusoidal SDW. The thermal factor is not included since it is negligible at small scattering angles. This equation gives S_{max}=0.09±0.01 μ_B/Fe, corresponding to S=0.06 μ_B/Fe root mean square value. The value of the ordered moment in BFO is ∼4 μ_B,[6] and therefore these values correspond to ∼1° canting of the Fe spins out of the plane of the cycloid.

Our measurements provide unambiguous evidence for the spin component normal to the plane of the cycloid. Since magnetic Bragg reflections are observed in the small-angle regime near $\mathbf{q} = \mathbf{0}$, this salient component must be ferromagnetically coupled in all directions. In

the direction of the cycloid propagation vector $\boldsymbol{\tau}$, the local ferromagnetism is modulated by the cycloidal periodicity and limited to $\sim$300 Å. In the other directions, the ferromagnetism extends, seemingly without bound, to macroscopic scales: at least 0.1 μm along the magnetization direction, and microns along [111]. Our neutron scattering measurements are not sensitive to the spin component parallel to $\boldsymbol{\tau}$, but from symmetry analyses,[8, 10] no ferromagnetically coupled spin components are expected in this direction. Thus, our experiments provide a strong evidence for the theoretically-predicted[8, 10] SDW shown in Fig 1(a), as well as for the associated local weak ferromagnetism in BFO.

Our results show that *intrinsic* weak ferromagnetism is possible in BFO films with suppressed spin cycloid, and provide a numerical estimate of the magnitude of the possible moment. BFO clearly holds promise for applications as a room-temperature ferromagnetic ferroelectric with coupled order parameters. Importantly, the observed magnetic moment is in the upper range of the theoretical predictions.[10, 11] Our results should provide an invaluable numerical input for realistic theoretical calculations of BFO's properties. In particular, the parameters characterizing the spin canting are crucial for understanding the dynamics of BFO, including the magnetic and hybrid excitations (electromagnons).[19–21] The associated dynamic magnetoelectric effects, such as giant changes of the magnon spectra in an electric field,[22] are of high current interest. It was proposed[19] that some of these effects could be used for electrical control of magnon propagation and for construction of spin-wave logical gates, emphasizing the importance of the interactions studied in this work.

In conclusion, we report observation of spin canting giving rise to local ferromagnetism in bulk $BiFeO_3$, confirming a long-standing theoretical prediction. The canting produces a spin density wave with the amplitude of 0.09 μ_B and spin direction normal to the plane of the magnetic cycloid. These results confirm possibility of *intrinsic* ferromagnetism in strained BFO, and provide numerical input necessary for understanding the giant magnetoelectric effects in this multiferroic material.

This work was supported by DOE DE-FG02-07ER46382 (V.K. and S.W.C.), and by the NSF under Grant No. DMR-1004568 (M.R.). It utilized facilities supported in part by NSF under Agreement No. DMR-0454672. M. L. acknowledges support from DanScatt.

[1] W. Eerenstein, N. D. Mathur, and J. F. Scott, Nature (London) **442**, 759 (2006); R. Ramesh and N. A. Spaldin, Nat. Mater. **6**, 13 (2007).

[2] For a review, see G. Catalan and J. F. Scott, Adv. Mater. **21**, 2463 (2009).

[3] I. Sosnowska, T. Peterlin-Neumaier and E. Steichele, J. Phys. C **15**, 4835 (1982).

[4] I. Sosnowska *et al.*, Physica B **180-181**, 117 (1992); R. Przenioslo *et al.*, J. Phys.: Condens. Matter **18**, 2069 (2006); J. Herrero-Albillos *et al., ibid.* **22**, 256001 (2010).

[5] S. Lee, T. Choi, W. Ratcliff II, R. Erwin, S-W. Cheong, V. Kiryukhin, Phys. Rev. B **78**, 100101(R) (2008); S. Lee, W. Ratcliff II, S-W. Cheong, V. Kiryukhin, Appl. Phys. Lett. **92**, 192906 (2008).

[6] D. Lebeugle, D. Colson, A. Forget, M. Viret, A. M. Bataille, A. Gukasov, Phys. Rev. Lett. **100**, 227602 (2008).

[7] T. Zhao, A. Scholl, F. Zavaliche, K. Lee, M. Barry, A. Doran, M. P. Cruz, Y. H. Chu, C. Ederer, N. A. Spaldin, R. R. Das, D. M. Kim, S. H. Baek, C. B. Eom, R. Ramesh, Nat. Mater. **5**, 823 (2006).

[8] A. M. Kadomtseva, A. K. Zvezdin, Yu. F. Popov, A. P. Pyatakov, G. P. Vorobev, JETP Lett. **79**, 571 (2004).

[9] D. Wardecki, R. Przenioslo, I. Sosnowska, Y. Skourski, M. Loewenhaupt, J. Phys. Soc. Japan **77**, 103709 (2008).

[10] C. Ederer and N. A. Spaldin, Phys. Rev. B **71**, 060401 (2005).

[11] D. Albrecht, S. Lisenkov, Wei Ren, D. Rahmedov, I. A. Kornev, L. Bellaiche, Phys. Rev. B **81**, 140401(R) (2010).

[12] J. Wang *et al.*, Science **299**, 1719 (2003).

[13] W. Eerenstein, F. D. Morrison, J. Dho, M. G. Blamire, J. F. Scott, N. D. Mathur, Science **307**, 1203a (2005).

[14] H. Béa, M. Bibes, A. Barthélémy, K. Bouzehouane, E. Jacquet, A. Khodan, J.-P. Contour, S. Fusil, F. Wyczisk, A. Forget, D. Lebeugle, D. Colson, M. Viret, Appl. Phys. Lett. **87**, 072508 (2005).

[15] M. Ramazanoglu, W. Ratcliff II, Y. J. Choi, S. Lee, S.-W. Cheong, V. Kiryukhin, Phys. Rev. B **83**, 174434 (2011).

[16] W. C. Chen, R. Erwin, J. W. McIver, S. Watson, C. B. Fu, T. R. Gentile, J. A. Borchers, J. W. Lynn, and G. L. Jones, Physica B **404**, 2663 (2009).

[17] R. M. Moon, T. Riste, and W. C. Koehler, Phys. Rev. **181**, 920 (1969).

[18] A. R. Wildes, Neutron News **17**, 17 (2006).

[19] R. de Sousa and J. E. Moore, Appl. Phys. Lett. **92**, 022514 (2008).

[20] D. Talbayev, S. A. Trugman, Seongsu Lee, Hee Taek Yi, S.-W. Cheong, A. J. Taylor, Phys. Rev. B **83**, 094403 (2011).

[21] M. Cazayous, Y. Gallais, A. Sacuto, R. de Sousa, D. Lebeugle, D. Colson, Phys. Rev. Lett. **101**, 037601 (2008).

[22] P. Rovillain, R. de Sousa, Y. Gallais, A. Sacuto, M. A. Measson, D. Colson, A. Forget, M. Bibes, A. Barthélémy, M. Cazayous, Nat. Mater. **9**, 975 (2010).